Improved Light Absorption of GaInP/GaAs/Ge Solar Cell Modules With Micro/ Nanoengineered Coverglasses

Eun Kyu Kang, Chan Il Yeo, Seok Jin Kang, Jung Wook Min, Young Min Song, and Yong Tak Lee

***Abstract*—We report on advanced types of coverglasses, which include the hierarchical micro- and subwavelength-structured surfaces for improved absorption efficiency of photovoltaic modules. Prism-shaped microstructures (PSMSs) help eliminate the optical shading caused by the metal grid of solar cells. The subwavelength structures (SWSs) with a tapered shape behave as a refractive index matching layer to reduce the surface reflection at the interface of air and coverglass. The geometries of the PSMSs and SWSs were designed by ray-tracing and the rigorous coupled-wave analysis method simulations, respectively, which provided the design guidelines. The PSMSs and SWSs were fabricated by a simple two-step process consisting of an isotropic wet etching process with hydrofluoric acid solution using a SiN_x mask and a self-masked dry etching process, respectively. A hybrid patterned coverglass incorporating the PSMSs with SWSs were mounted on GaInP/(In)GaAs/Ge triple-junction solar cells with a precise alignment process. The measured power conversion efficiency of the subreceiver module with the patterned glass reached 32.97% for 1 sun, which is 11.19% higher compared with a subreceiver module with a flat coverglass.**

***Index Terms*—Coverglasses, microstructure, self-masked dry etching (SMDE), solar cells, subwavelength structure.**

I. Introduction

COMPOUND semiconductor multijunction (MJ) solar cells are the attractive choice for space and terrestrial application due to their high efficiency (obtained by stacking materials of different bandgap), excellent lifetime/reliability, and favorable manufacturing costs [1]–[5]. However, their performance in commercially available cells still has not reached the theoretical limit. As a result, research on compound semiconductor-based solar cells often focuses on three categories: 1) optimizing multiple layer stacking by bandgap engineering, 2) effective photocurrent extraction by fine tuning the metal grid design, and 3) micro- or nanoengineered geometry for managing light absorption. To be effective in converting the incident photons to electricity, all these issues need to be considered simultaneously and without producing detrimental effects on each features.

For example, one instance is the relation between optical and electrical properties determined by the metal grid lines. Finely designed front metal grids, which effectively extract the generated photocurrent, occupy approximately 10–15% of the surface area of the III–V-based MJ solar cell [6]–[8]. However, the metal grids also result in optical shadowing, which causes a decline in the power conversion efficiency (PCE) of the solar cells. Therefore, light management is necessary to guide the incident sunlight to avoid the metal grid area, to reduce the metal grid optical losses and thereby improve the PCE of III–V-based MJ solar cell with solar tracking system and concentrator [9]. In previous studies, cylindrical microstructures patterned cover materials were used to reduce the shadowing effect caused by metal grids [10]–[12]. However, these cover materials did not eliminate the Fresnel reflection of front surface. In order to boost the module PCE, the preferred light management structure should also include broadband antireflection properties [13]–[14].

In this report, we present an optical management technique to reduce optical losses using advanced coverglasses, including prism-shaped microstructures (PSMSs) and subwavelength structures (SWSs). The light incidence angle was controlled using PSMSs so that all light incident to the coverglass could be propagated to the solar cell, avoiding the metal grid. In other words, the optical loss produced by the metal grids due to its shadowing effect is decreased by the PSMSs. In addition, broadband antireflection structures (BARSs) [15] on the cover surface such as SWSs can solve the refractive index mismatch problem.

Hybrid (PSMS/SWSs) structures (HSs) patterned coverglass (HSC) capable of reducing two types of optical losses were fabricated using simple wet and dry etching [16]–[17]. First, a PSMS array with 4-μm height and 20-μm width was fabricated using isotropic wet-etching process with 49% hydrofluoric (HF) solution. Then, a self-masked dry etching (SMDE) process was used to form the SWSs over the entire surface. The detailed mechanism of the SMDE process is explained in our previous study [18]. The HSC was mounted using a flip-chip bonder (Fineplacer femto) with a precise alignment process; misalignment is closely related to optical loss [19]. Silicone resin was used for the adhesive layer in the mounting process, since the refractive index of the silicone resin is similar to glass [20]. As

Manuscript received February 24, 2015; revised April 1, 2015; accepted April 22, 2015. Date of publication May 7, 2015; date of current version June 18, 2015. This work was supported by the National Research Foundation of Korea (NRF) grant funded by the Korea government (MEST) (No. 2011-0017606) and by the Agency for Defense Development (UE135157OD), Republic of Korea.

E. K. Kang, C. I. Yeo, and S. J. Kang are with the School of Information and Communications, Gwangju Institute of Science and Technology, Gwangju 500-712, Korea (e-mail: ekkang@gist.ac.kr; ciyeo@gist.ac.kr; seokjin@gist.ac.kr).

J. W. Min is with the Department of Physics and Photon Science, Gwangju Institute of Science and Technology, Gwangju 500-712, Korea (e-mail: jwmin@gist.ac.kr).

Y. M. Song is with the Department of Electronic Engineering, Pusan National University, Busan 609-735, Korea (e-mail: ymsong81@gmail.com).

Y. T. Lee is with the School of Information and Communications and Advanced Photonics Research Institute, Gwangju Institute of Science and Technology, Gwangju 500-712, Korea (e-mail: ytlee@gist.ac.kr).

Color versions of one or more of the figures in this paper are available online at http://ieeexplore.ieee.org.

Digital Object Identifier 10.1109/JPHOTOV.2015.2426505

2156-3381 © 2015 IEEE. Personal use is permitted, but republication/redistribution requires IEEE permission.
See http://www.ieee.org/publications_standards/publications/rights/index.html for more information.

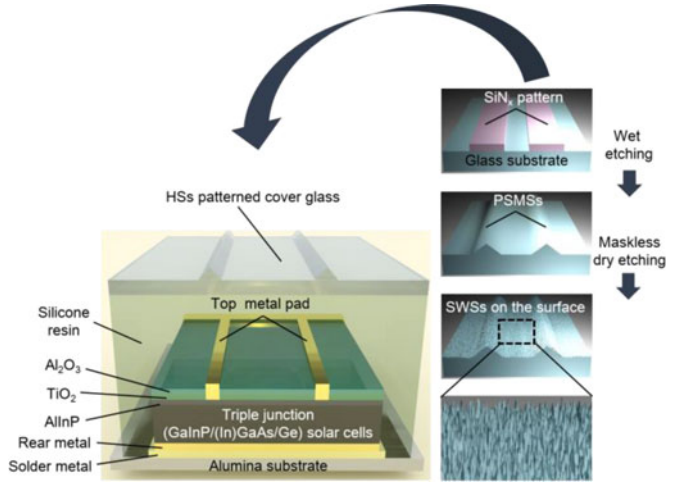

Fig. 1. Schematic illustration of cross-sectional view of TJ GaInP/(In)GaAs/Ge solar cell with HSs patterned coverglass. The right figures show process steps for fabricating the HSs patterned coverglass.

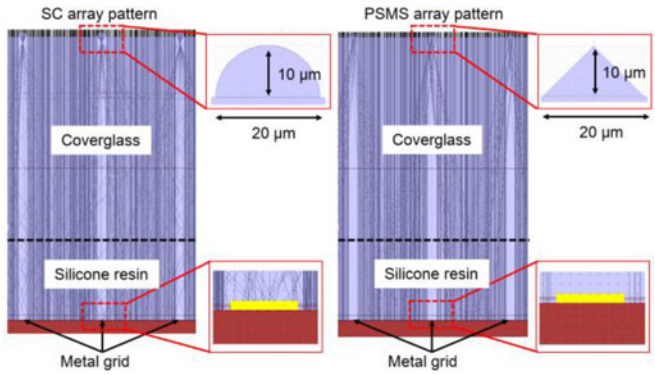

Fig. 2. Ray-tracing simulation of SC patterned coverglass and PSMSC with the metal grid of a solar cells.

a result, reflection loss was minimized at the interface of the coverglass and the top surface of the solar cells.

The simply fabricated HSC has two functions: the PSMSs can effectively refract light due to their geometrical shape, and the SWSs also reduce light reflection by acting as a refractive index matching layer at the interface between air ($n = 1.00$) and coverglass ($n = 1.47$) [20]. Before fabricating the HSC, theoretical calculations based on ray-tracing [21] and rigorous coupled-wave analysis (RCWA) method [22] was utilized as guidance for determining the geometrical effect of the PSMSs and SWSs, respectively. The optical properties of the HSC were investigated by transmittance spectra measurement and were confirmed by the characterization of the coverglass mounted solar cells.

II. Experimental Details

Fig. 1 shows the schematic of the triple-junction (TJ) GaInP/(In)GaAs/Ge solar cell with HSC. In this experiment, the solar cell (active area = 0.25 mm^2) consists of a TiO_2/Al_2O_3 double layer antireflection coating and top metal grid having a width of 17 μm and a period of 163 μm. The solar cell was mounted on an alumina substrate with a gold-plated thick copper electrode using cream-type solder ($Sn_{96.5}/Ag_{3.0}/Cu_{0.5}$ alloy metal). The soldering process was carried out on a hot plate at 260 °C. Then, the solar cell was encapsulated by a silicone resin and the HSC was mounted on the top of the silicone resin using the flip-chip bonder. After that, the silicone resin hardening process was performed at 150 °C for 5 min.

The HSC fabrication steps are described in the right image of Fig. 1. First, a 1-μm-thick SiN_x layer was deposited on the coverglass substrate (BoroFloat 33, Schott) using plasma-enhanced chemical vapor deposition, and a conventional photolithography process was performed to form mask patterns. The photoresist (PR) patterns had a width of 30 μm so as to overlap the top metal grid of the solar cell. The period of the pattern was 163 μm. SiN_x was dry etched using RIE with CF_4 (30 sccm), rf power of 100 W, and process pressure of 100 mTorr for 20 min. After the RIE process, the remaining PR was removed in acetone with ultrasonic agitator. The flat coverglass (FC) with SiN_x etching mask was dipped into the 49% HF solution at room temperature for 240 s. Surface morphologies of the fabricated coverglass were characterized by a field-emission scanning electron microscope (FE-SEM, Hitachi 4700).

PSMSs were formed by isotropically wet etching the glass in HF solution. Then, SWSs with tapered profiles were formed on the PSMS array patterned cover glass (PSMSC) using the SMDE method, under optimum RIE conditions, i.e., CF_4/O_2 (40/10 sccm) with rf power of 50 W, and process pressure of 50 mTorr for 7 min. After the SMDE process, the coverglass was cleaned using acetone/methanol/deionized water for 3 min, respectively. The SWSs were uniformly formed on the entire surface of the PSMSC.

The transmittance of the fabricated SWSs patterned coverglass (SWSC), PSMSC, and HSC were evaluated from 400- to 1800-nm wavelength, using a spectrophotometer (Cary 500, Varian) with an integrating sphere. Three kinds of coverglass with an area of 30 mm^2 were mounted on solar cells having similar properties using a flip-chip bonder. The PSMSs and HSs patterns were precisely aligned with the metal grid of the solar cells because any misalignment strongly reduces the PCE of the solar cells module. Current density–voltage (J–V) characteristics of the coverglass mounted solar cells were measured using a solar simulator (Sol3A, Oriel, USA) under AM 1.5G (1000 W/m^2) irradiation at room temperature.

III. Results and Discussion

A. Optical Simulations and Fabrications

Prior to fabricating the HSC, theoretical calculations were conducted to determine the geometrical features of HSs that result in desired properties. Ray-tracing and a RCWA method were used to obtain the desirable micro- and nanostructures because of the limited time and resources available for each simulation tool [21]. To determine a desirable microstructure, a semicylinder (SC) array and a PSMS array with 20-μm width and 10-μm height were considered. In this simulation, the thickness of the

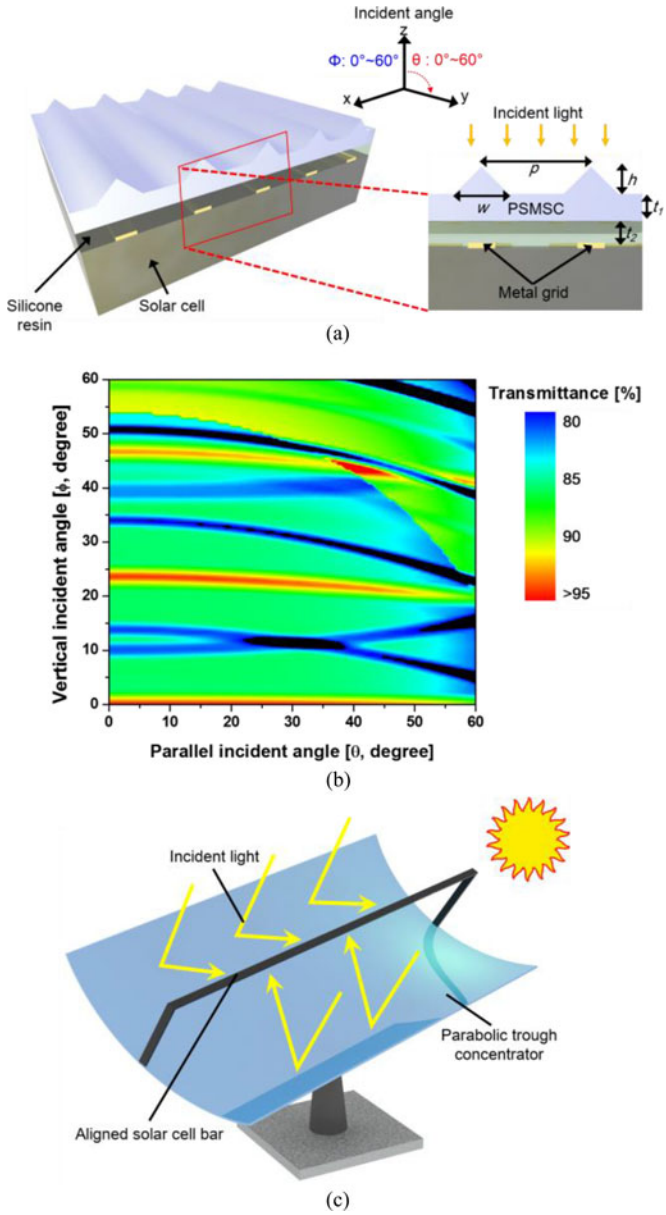

Fig. 3. (a) Schematic illustration of a model to calculate incident angle-dependent transmittance of PSMSC as a function of θ and Φ. The inset on the right shows an enlarged cross-sectional view. (b) Contour plot of calculated effective transmittance of PSMSC in detail. In these calculations, the geometry of the PSMSC was fixed as $p = 163\ \mu$m, $h = 4.5\ \mu$m, $w = 20\ \mu$m, $t_1 = 500\ \mu$m, and $t_2 = 150\ \mu$m. (c) Schematic illustration of a solar tracking system and a parabolic trough concentrator.

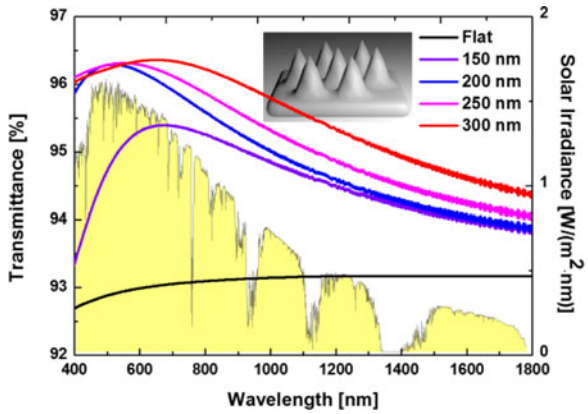

Fig. 4. Calculated transmittance of SWSC as a function of height of SWSs in the wavelength range from 300 to 1800 nm using the RCWA method. Inset indicates a calculation model.

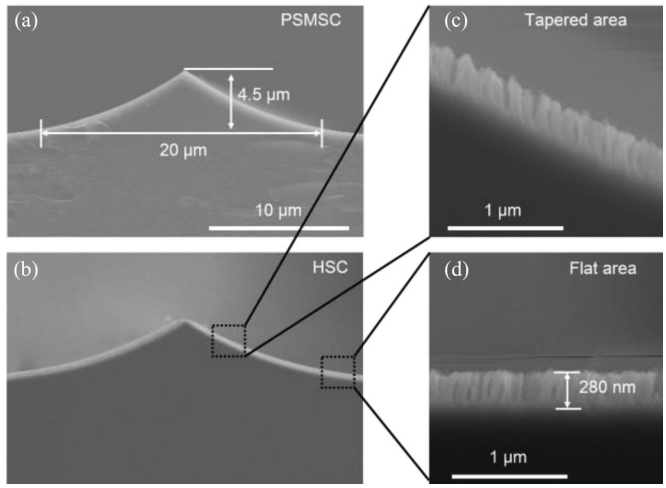

Fig. 5. SEM image of cross-sectional view of fabricated HSC. (a) Fabricated PSMS has 4.5-μm height, 20-μm width, and a tapered profile. (b) SWSs formed on PSMS using the SMDE process. (c) Magnified view of inclined area of HSC. (d) Magnified view of flat area of HSC.

glass ($n = 1.47$) and silicone resin ($n = 1.50$) were fixed at 500 and 150 μm, respectively. Optical properties of the metal grid with 17-μm width were set to have 50% reflection and 50% absorption at a wavelength of 550 nm. Fig. 2 shows that the PSMS was more effective in increasing the light absorption of the solar cell compared to the SC. The light incident at the top area of the SC had a small angle of refraction, while light rays that were incident at the edges of the SC had a larger angle of refraction [23]. Therefore, for the SC structure, some of the light rays were incident on the metal grids, while for the PSMS, none of the refracted rays were incident on the metal grids due to their similar refracting angle.

The incident angle-dependent transmittance of the PSMSC was also calculated since in a practical solar energy system, the incident angle of sunlight changes with season and time. In the calculations, θ (parallel incident angle) and Φ (vertical incident angle) were changed from 0° to 60°. Fig. 3(a) and (b) shows the simulation model and the calculated transmittance of the PSMSC, respectively. The transmittance of the PSMSC was influenced by variations in the vertical incident angle, while it remained unaffected by variations in the parallel incident angle. Nonetheless, the vertical incident angle-dependent transmittance of PSMSC can be minimized by using a solar tracking system and a parabolic trough concentrator [24], [25] because the direction of installation of the solar module with PSMSC can be controlled as shown Fig. 3(c).

To further increase transmittance by suppressing approximately 4% of the surface reflection loss (Fresnel reflection loss)

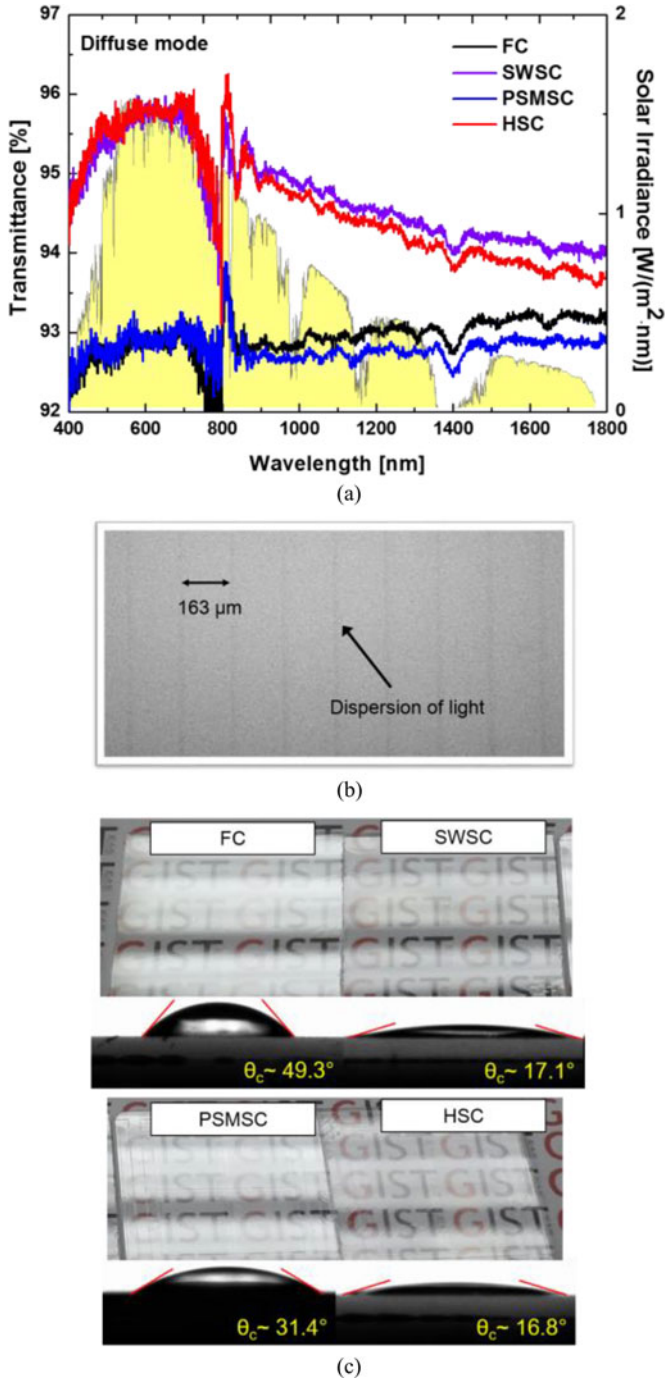

Fig. 6. (a) Measured transmittance of four difference coverglasses in the wavelength range from 400 to 1800 nm. (b) CCD image of PSMSC using white backlight. (c) FC, SWSC, PSMSC, and HSC under fluorescent light. Water droplet on fabricated coverglass with corresponding contact angle.

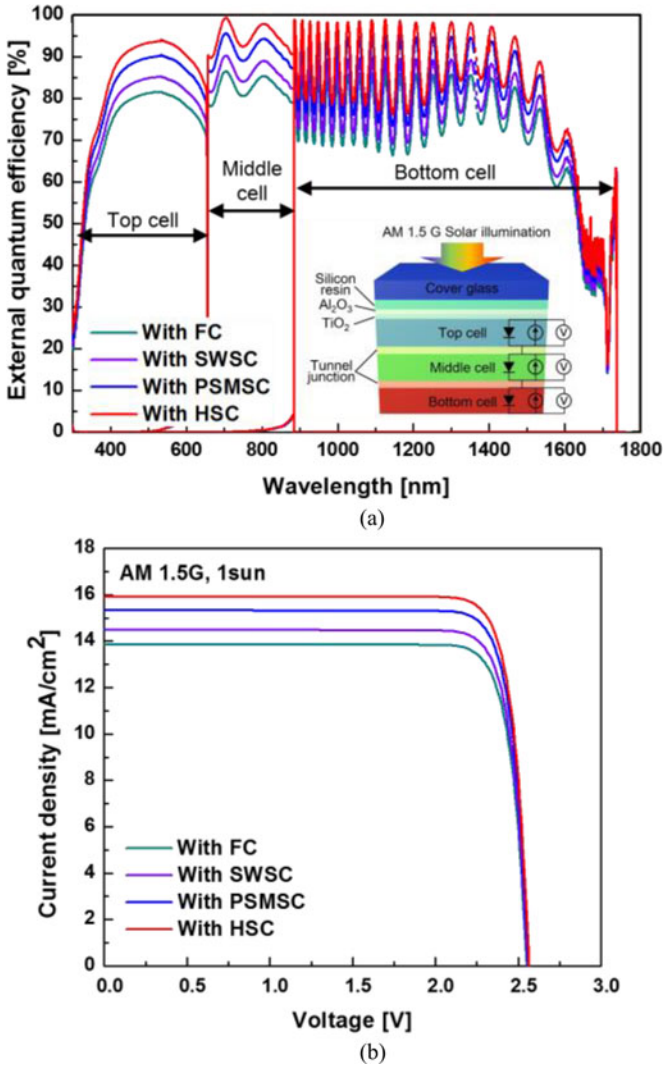

Fig. 7. (a) Calculated EQE of the TJ solar cells with four different coverglasses. Inset indicates a calculated model. (b) *J–V* characteristics of solar cells with four different types of coverglasses under AM 1.5G (1000 W/m^2) irradiation.

TABLE I
SIMULATED DEVICE CHARACTERISTICS OF THE SOLAR CELL FOR FOUR TYPES OF COVERGLASSES

	V_{oc} (V)	J_{sc} (mA/cm^2)	Fill Factor (%)	Efficiency (%)
With FC	2.55	13.86	85.55	30.16
With SWSC	2.55	14.47	85.56	31.57
With PSMSC	2.56	15.31	85.64	33.56
With HSC	2.56	15.92	85.65	34.87

due to the difference in refractive index between air and coverglass, SWSs were employed like BARs on the top surface of the coverglass. Fig. 4 shows the calculated transmittance of SWSs with a period of 100 nm and a width of 100 nm as a function of their heights (0, 150, 200, 250, 300 nm) in the wavelength range from 300 to 1800 nm using the RCWA method. The calculated transmittance of the FC is also shown for comparison. The FC exhibits transmittance of ~93% at all wavelengths of the spectrum. In contrast, the SWSCs transmittance tends to increase, particularly at short wavelengths (i.e., visible wavelengths). The transmission spectrum of the SWSC is more favorable for enhancing the transmittance of sunlight into the solar cell, as can be seen in Fig. 4.

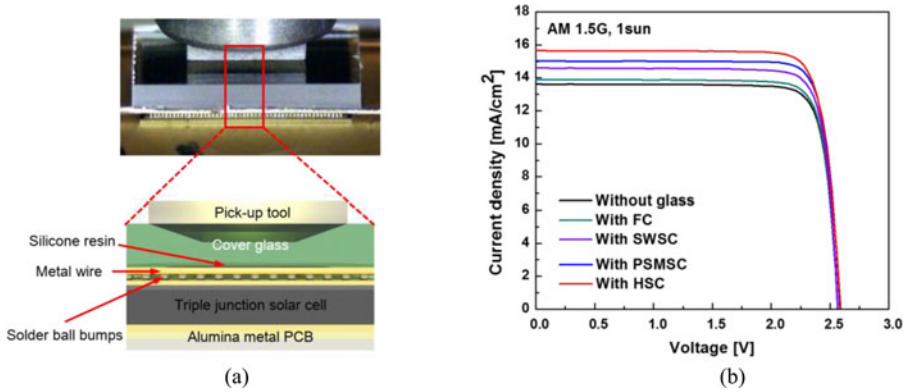

Fig. 8. (a) Process for mounting coverglass to solar cell using flip-chip bonder. The inset on the bottom shows a cross sectional view. (b) *J–V* characteristics of solar cells without glass and with four different types of coverglasses under AM 1.5G (1000 W/m^2) irradiation.

The HSC was fabricated using parameters based on calculation results. Fig. 5(a) and (b) shows SEM images of the cross-sectional view of the fabricated PSMSC and HSC, respectively. The fabricated PSMSs have approximately 4.4-μm height, 20-μm width, and 35° slope of the tangent. SWSs with 270–280 nm height, 80–100 nm width, and 80–100 nm period were uniformly formed on the entire surface of the coverglass as shown in Fig. 5(c) and (d). The SMDE process used in this study is very useful for forming SWSs on an uneven surface because the nanoscale mask is generated by the reaction between the etching gas and material during the etching process.

Fig. 6(a) shows the measured transmittance spectra of four different types of coverglasses at wavelengths of 300–1800 nm. As expected, the SWSC and HSC increased the transmittance from ∼93% (i.e., transmittance of the FC) up to ∼96%. It is observed that the transmittance of the PSMSs were almost the same as the FC at short wavelengths (400–1000 nm) because the bottom side of fabricated coverglass does not include the metal grids. Therefore, the transmission enhancement due to the presence of microstructure is not apparent in Fig. 6(a). The spike near 800-nm wavelength was produced as a result of changing the source and detector in the UV-Vis-NIR spectrophotometer during the measurement.

To confirm the light guiding effect of the PSMSs, a charge-coupled device (CCD) camera and white backlight were used [26]. Fig. 6(b) shows the dispersion of light in PSMSC. The dark area in the figure is the PSMSs patterned region on the PSMSC, which means that the light incident on the metal grid can be refracted by the PSMSs. Therefore, the effective transmittance can be enhanced by eliminating the shadowing effect. The difference of reflectance and wetting properties in FC and three different types of coverglasses is displayed in Fig. 6(c). After wet and dry etching of glasses, contact angle (θ_c) of a liquid droplet is changed due to the surface energy changes [27]. The contact angle measurement system (Phoenix-300 Touch, SEO Co., Ltd., Korea) was used to measure the contact angle of a water droplet. The three etched glasses (SWSC: $\theta_c \sim 17.1°$, PSMSC: $\theta_c \sim 31.4°$, and HSC: $\theta_c \sim 16.8°$) exhibited improved hydrophilicity compared with that of FC glass ($\theta_c \sim 49.3$) due to chemical treatment (HF, CF_4, O_2) and surface roughness. Hydrophilic properties of glass surface can provide the self-cleaning function [28]–[30].

B. Calculation of External Quantum Efficiency

Silvaco simulation was conducted to confirm the enhancement of external quantum efficiency (EQE) and short-circuit current density (J_{sc}). In the simulation, the optical calculation results obtained by Lightools simulation are utilized as transmittance of each glass. For the simulation, the incident angle is assumed to be normal since the change in the incident angle as the light rays pass through PSMSC is negligibly small. In Fig. 7(a), four types of coverglasses are incorporated to TJ solar cells, and among them, HSC shows the highest EQE. Fig. 7(b) shows the *J–V* curves of four types of coverglasses. Since the amount of light that is transmitted is determined by the coverglasses, J_{sc} that has linear relation with number of absorbed photons is greatly affected by the effective enhancement in the light transmission. Table I shows the detailed characteristics of TJ solar cells with different types of coverglasses. The TJ solar cells with the HSC showed the highest J_{sc} of 15.92 mA/cm^2 and PCE of 34.87%. The J_{sc} and PCE of the solar cell module with HSC is enhanced by 14.86% and 15.61%, respectively, compared with that of the solar cell module with the FC.

C. Device Characteristics of the Fabricated Solar Cells

To determine the effect of the four types of coverglasses on solar cell performance, the fabricated coverglasses were mounted on the TJ solar cells using a flip-chip bonder with silicone resin. In this experiment, TJ solar cells that had similar performance without a coverglass were selected in order to avoid any interference arising from the solar cell itself. Fig. 8(a) shows the mounting process using a flip-chip bonder. Solder balls were placed on the n-metal using laser solder jetting system (SB2-Jet). Then, the metal wire (Cu) was placed on the solder ball with thermal process at 200 °C to contact n-type metal and metal pad of the alumina substrate. Silicone-resin-coated solar cell module was loaded in the flip-chip bonder. The coverglass was lifted by the pick-up tool of the flip chip bonder. After precise alignment (metal grids and PSMSs), each coverglass was mounted

TABLE II
DEVICE CHARACTERISTICS OF THE SOLAR CELL FOR FIVE DIFFERENT TYPES OF COVERGLASSES

	V_{oc} (V)	J_{sc} (mA/cm^2)	Fill Factor (%)	Efficiency (%)	Enhancement ratio (%)
Without glass	2.54	13.60	83.82	28.95	-
With FC	2.54	13.91	83.93	29.65	2.41
With SWSC	2.54	14.57	83.71	30.97	6.97
With PSMSC	2.55	15.00	83.90	32.09	10.84
With HSC	2.55	15.60	82.91	32.97	13.88

on the TJ solar cells and was bonded with silicone resin using the thermal hardening process.

The measured *J–V* curves of the solar cell modules without coverglass and with four different types of coverglasses under AM 1.5G (1000 W/m^2) irradiation at normal incidence are presented in Fig. 8(b). To establish the reliability of the measurement results, the performance of each sample was measured five times and averaged. The obtained device characteristics are summarized in Table II. The solar cell module without a coverglass exhibited a J_{sc} of 13.60 mA/cm^2 and a PEC of 28.95%. The J_{sc} and PEC were slightly enhanced by incorporating the FC, to 13.91 mA/cm^2 and 29.65%, respectively, due to the refractive index matching of the coverglass ($n = 1.47$) between air ($n = 1.00$) and Al_2O_3 ($n = 1.80$).

The solar cell modules with patterned coverglasses showed significantly enhanced J_{sc} and PEC compared with the module with the FC. Among them, the solar cell module with the HSC showed the highest J_{sc} of 15.60 mA/cm^2 and PCE of 32.97%. The J_{sc} and PCE is enhanced by 12.14% and 11.19%, respectively, compared with that of the solar cell module with the FC, due to the efficient light management. The open-circuit voltage (V_{oc}) and the fill factor remained similar.

IV. CONCLUSION

An advanced HSC was fabricated by isotropic wet etching and SMDE processes to enhance the PCE of a GaInP/(In)GaAs/Ge TJ solar cell. Optical characteristics of the fabricated SWSC, PSMSC, and HSC were investigated as a function of wavelength. Theoretical calculations were conducted using ray-tracing and RCWA method to provide fabrication guidelines. The TJ solar cells with HSC exhibited greatly enhanced photovoltaic performance as a result of both the elimination of optical shadowing and the reduction of surface reflection by PSMSs and SWSs, respectively. From these results, we expect that HSC have promising potential for improving the performance of various photovoltaic devices.

ACKNOWLEDGEMENT

The authors would like to acknowledge Mr. S. Ravindran at GIST for his fruitful comments and suggestions.

REFERENCES

[1] K. W. J. Barnham, M. Mazzer, and B. Clive, "Resolving the energy crisis: Nuclear or photovoltaics?" *Nat. Mater.*, vol. 5, no. 3, pp. 161–164, 2006.
[2] M. Yamaguchi, "III–V compound multi-junction solar cells: Present and future," *Sol. Energy Mater. Sol. Cells*, vol. 75, no. 1, pp. 261–269, 2003.
[3] A. Luque, "Will we exceed 50% efficiency in photovoltaics?" *J. Appl. Phys.*, vol. 110, no. 3, p. 031301, 2011.
[4] M. A. Cappelletti, A. P. Cédola, and E. P. y Blancá, "Computational analysis of the maximum power point for GaAs sub-cells in InGaP/GaAs/Ge triple-junction space solar cells," *Semicond. Sci. Technol.*, vol. 29, no. 11, p. 115025, 2014.
[5] D. C. Law, R. R. King, H. Yoon, M. J. Archer, A. Boca, C. M. Fetzer, S. Mesropian, T. Isshiki, M. Haddad, K. M. Edmondson, D. Bhusari, J. Yena, R. A. Sherif, H. A. Atwater, and N. H. Karam, "Future technology pathways of terrestrial III–V multijunction solar cells for concentrator photovoltaic systems," *Sol. Energy Mater. Sol. Cells*, vol. 94, no. 8, pp. 1314–1318, 2010.
[6] H. Cotal, C. Fetzer, J. Boisvert, G. Kinsey, R. King, P. Hebert, H. Yoon, and N. Karam, "III–V multijunction solar cells for concentrating photovoltaics," *Energy Environ. Sci.*, vol. 2, no. 2, pp. 174–192, 2009.
[7] A. Antonini, M. Stefancich, D. Vincenzi, C. Malagu, F. Bizzi, A. Ronzoni, and G. Martinelli, "Contact grid optimization methodology for front contact concentration solar cells," *Sol. Energy Mater. Sol. Cells*, vol. 80, no. 2, pp. 155–166, 2003.
[8] K. Nishioka, T. Takamoto, T. Agui, M. Kaneiwa, Y. Uraoka, and T. Fuyuki, "Evaluation of InGaP/InGaAs/Ge triple-junction solar cell and optimization of solar cell's structure focusing on series resistance for high-efficiency concentrator photovoltaic systems," *Sol. Energy Mater. Sol. Cells*, vol. 90, no. 9, pp. 1308–1321, 2006.
[9] G. Zubi, J. L. Bernal-Agustín, and G. V. Fracastoro, "High concentration photovoltaic systems applying III–V cells," *Renew. Sustain. Energy Rev.*, vol. 13, no. 9, pp. 2645–2652, 2009.
[10] S. Dal Zilio, K. Tvingstedt, O. Inganäs, and M. Tormen, "Fabrication of a light trapping system for organic solar cells," *Microelectron. Eng.*, vol. 86, no. 4, pp. 1150–1154, 2009.
[11] O. Korech, J. M. Gordon, E. A. Katz, D. Feuermann, and N. Eisenberg, "Dielectric microconcentrators for efficiency enhancement in concentrator solar cells," *Opt. Lett.*, vol. 32, no. 19, pp. 2789–2791, 2007.
[12] A. Boca, K. M. Edmondson, and R. R. King, "Prismatic covers for boosting the efficiency of high-concentration PV systems," in *Proc. 34th IEEE Photovoltaic Spec. Conf.*, 2009, pp. 000131–000136.
[13] G. C. Park, Y. M. Song, E. K. Kang, and Y. T. Lee, "Size-dependent optical behavior of disordered nanostructures on glass substrates," *Appl. Opt.*, vol. 51, no. 24, pp. 5890–5896, 2012.
[14] Y. M. Song, Y. Jeong, C. I. Yeo, and Y. T. Lee, "Enhanced power generation in concentrated photovoltaics using broadband antireflective coverglasses with moth eye structures," *Opt. Exp.*, vol. 20, no. 106, pp. A916–A923, 2012.
[15] Y.-F. Huang, S. Chattopadhyay, Y.-J. Jen, C.-Y. Peng, T.-A. Liu, Y.-K. Hsu, C.-L. Pan, H.-C. Lo, C.-H. Hsu, Y.-H. Chang, C.-S. Lee, K.-H. Chen, and L.-C. Chen, "Improved broadband and quasi-omnidirectional anti-reflection properties with biomimetic silicon nanostructures," *Nat. Nanotechnol.*, vol. 2, no. 12, pp. 770–774, 2007.
[16] N. Pekas, Q. Zhang, M. Nannini, and D. Juncker, "Wet-etching of structures with straight facets and adjustable taper into glass substrates," *Lab. Chip*, vol. 10, no. 4, pp. 494–498, 2010.
[17] T. Corman, P. Enoksson, and G. Stemme, "Deep wet etching of borosilicate glass using an anodically bonded silicon substrate as mask," *J. Micromech. Microeng.*, vol. 8, no. 2, p. 84, 1998.
[18] Y. M. Song, G. C. Park, E. K. Kang, C. I. Yeo, and Y. T. Lee, "Antireflective grassy surface on glass substrates with self-masked dry etching," *Nanoscale Res. Lett.*, vol. 8, no. 1, pp. 1–5, 2013.
[19] M. Nam, K. Kim, J. Lee, K.-K. Lee, and S. S. Yang, "Concentrating microlens array mounted on an InGaP/GaAs/Ge solar cell for photovoltaic performance enhancement," *Sol. Energy*, vol. 91, pp. 374–380, 2013.
[20] E. F. Schubert, T. Gessmann, and J. K. Kim, *Light Emitting Diodes*. New York, NY, USA: Wiley, 2005.
[21] E. K. Kang, Y. M. Song, S. J. Jang, C. I. Yeo, and Y. T. Lee, "Increased light extraction from GaN light-emitting diodes by SiN_x compound eyes," *IEEE Photon. Technol. Lett.*, vol. 25, no. 12, pp. 1118–1121, Jun. 2013.
[22] T. Schuster, J. Ruoff, N. Kerwien, S. Rafler, and W. Osten, "Normal vector method for convergence improvement using the RCWA for crossed gratings," *J. Opt. Soc. Amer. A*, vol. 24, no. 9, pp. 2880–2890, 2007.

[23] F. L. Pedrotti and L. S. Pedrotti, *Introduction to Optics*, vol. 1, 2nd ed. Englewood Cliffs, NJ, USA: Prentice Hall, 1993.
[24] D. Vallentin and P. Viebahn, "Economic opportunities resulting from a global deployment of concentrated solar power (CSP) technologies—The example of German technology providers," *Energy Policy*, vol. 38, no. 8, pp. 4467–4478, 2010.
[25] V. A. Salomoni, A. Miliozzi, C. E. Majorana, D. Nicolini, and G. M. Giannuzzi, *New Trends in Designing Parabolic Trough Solar Concentrators and Heat Storage Concrete Systems in Solar Power Plants*. Rijeka, Croatia: InTech, 2010.
[26] M. Nam, H. Oh, H. Seo, Y. Song, S. Yang, and K. Lee, "Development of a polymer coating-based microlens array on isotropically wet-etched quartz substrates for maskless lithography application," *Jpn. J. Appl. Phys.*, vol. 49, no. 6S, p. 06GN10, 2010.
[27] J. Blass, O. Köhler, M. Fingerle, C. Müller, and C. Ziegler, "Properties and characteristics of wet (HF) and dry (RIE) etched borosilicate glass," *Phys. Status Solidi A*, vol. 210, no. 5, pp. 988–993, 2013.
[28] J. Son, S. Kundu, L. K. Verma, M. Sakhuja, A. J. Danner, C. S. Bhatia, and H. Yang, "A practical superhydrophilic self cleaning and antireflective surface for outdoor photovoltaic applications," *Sol. Energy Mater. Sol. Cells*, vol. 98, pp. 46–51, 2012.
[29] L. K. Verma, M. Sakhuja, J. Son, A. J. Danner, H. Yang, H. C. Zeng, and C. S. Bhatia, "Self-cleaning and antireflective packaging glass for solar modules," *Renew. Energy*, vol. 36, no. 9, pp. 2489–2493, 2011.
[30] C. I. Yeo, E. K. Kang, S. K. Lee, Y. M. Song, and Y. T. Lee, "Efficiency enhancement of III-V triple-junction solar cell using nanostructured bifunctional coverglass with enhanced transmittance and self-cleaning property," *IEEE Photon. J.*, vol. 6, no. 3, art. no. 8400209, Jun. 2014.

Authors' photographs and biographies not available at the time of publication.